Live Cell Imaging

International Edition: DOI: 10.1002/anie.201703406
German Edition: DOI: 10.1002/ange.201703406

# Localized Chemical Remodeling for Live Cell Imaging of Protein-Specific Glycoform

*Jingjing Hui, Lei Bao, Siqiao Li, Yi Zhang, Yimei Feng, Lin Ding,* and Huangxian Ju**

***Abstract:*** *Live cell imaging of protein-specific glycoforms is important for the elucidation of glycosylation mechanisms and identification of disease states. The currently used metabolic oligosaccharide engineering (MOE) technology permits routinely global chemical remodeling (GCM) for carbohydrate site of interest, but can exert unnecessary whole-cell scale perturbation and generate unpredictable metabolic efficiency issue. A localized chemical remodeling (LCM) strategy for efficient and reliable access to protein-specific glycoform information is reported. The proof-of-concept protocol developed for MUC1-specific terminal galactose/N-acetylgalactosamine (Gal/GalNAc) combines affinity binding, off-on switchable catalytic activity, and proximity catalysis to create a reactive handle for bioorthogonal labeling and imaging. Noteworthy assay features associated with LCM as compared with MOE include minimum target cell perturbation, short reaction timeframe, effectiveness as a molecular ruler, and quantitative analysis capability.*

Protein glycosylation is a ubiquitous post-translational, diversity-generating covalent modification process.[1] The glycosylation pattern of a protein, as characterized by the population of glycoforms, is subject to elaborate control by cellular synthetic machinery[2a] and in turn, defines the biological functions of a protein[2b] and the recognition and signaling properties of a cell.[2c] A hallmark of protein glycosylation is its highly dynamic and adaptive nature in response to the physiological state of a cell.[1,3] Live cell imaging of protein-specific glycoform in an in situ fashion can therefore not only help to advance the understanding of glycosylation pathways and functions but also provide a potentially working channel for diagnostic and therapeutic usage.[4]

Metabolic oligosaccharide engineering (MOE) has been the tour de force tool developed for glycoform imaging.[5] This ingenious approach permits system-level incorporation of reactive unnatural carbohydrate moiety for subsequent bioorthogonal elaboration with one assay probe,[4] and protein-specific tagging of the other probe is achieved through either protein fusion[4a,b] or affinity binding;[4c,d] a distance-dependent physical process between two probes, such as Förster resonance energy transfer, is then used to confine detection to the intra-glycoprotein spacing level and can therefore report on the glycoform associated with a particular protein.[4] However, despite the exciting progress witnessed in this promising field, drawbacks are apparent when using MOE as a protein-specific glycoform imaging tool. MOE is a non-selective, global chemical remodeling (GCM) technology exerting unnecessary perturbation on the whole-cell scale, which creates essentially a cell in a different physiological state, and therefore, the originally targeted native cell is no longer available for examination. Although tolerance of unnatural carbohydrate analogue at the enzyme level is clear, metabolic delivery at the cellular level is a complex, poorly understood process, leading inevitably to unpredictable metabolic efficiency and installation percentage issues.[6] This unpredictability renders it problematic to translate glycoform data acquired on a cell in its metabolically altered state to the corresponding information for the native cell and as a consequence, comparison among cells in different physiological states and across cell lines can become a formidable challenge.

With these inadequacies in mind, we embarked on an endeavor to develop a protein-specific imaging strategy that both minimizes perturbation on the cell and allows straightforward interpretation of the glycoform data. Ideally, the perturbation should be applied only at the to-be-probed carbohydrate site of interest, and glycoform information acquired through a well-defined chemical transformation can be representative of and proportionally extrapolated to the whole protein-specific target glycoform population. Herein we present a localized chemical remodeling (LCM) method for live cell imaging of protein-specific glycoform (Scheme 1). This method relies on a combination of affinity binding, off-on switchable catalytic activity, and proximity catalysis to create a reactive handle for bioorthogonal labeling and imaging. Instead of relying on a physical process, LCM essentially provides a molecular ruler that can report on intramolecular distance by using chemical reactivity as a reporter system.

As a proof-of-concept demonstration, we selected MUC1-bound terminal galactose/*N*-acetylgalactosamine (Gal/GalNAc) as the imaging target. MUC1 is a transmembrane glycoprotein that contains an extracellular, heavily *O*-glycosylated variable number tandem repeat (VNTR) domain.[7a] Aberrant MUC1 glycosylation invariably observed in human epithelial cancer cells has established its utility as a highly sensitive diagnostic and prognostic cancer biomarker.[7b] Gal/GalNAc termini have been implicated as recognition determinants governing both normal physiological functions and

[*] J. Hui, L. Bao, S. Li, Y. Zhang, Y. Feng, Prof. Dr. L. Ding, Prof. Dr. H. Ju
State Key Laboratory of Analytical Chemistry for Life Science
School of Chemistry and Chemical Engineering
Nanjing University, Nanjing 210023 (P.R. China)
E-mail: dinglin@nju.edu.cn
hxju@nju.edu.cn
Supporting information and the ORCID identification number(s) for the author(s) of this article can be found under: https://doi.org/10.1002/anie.201703406.

  

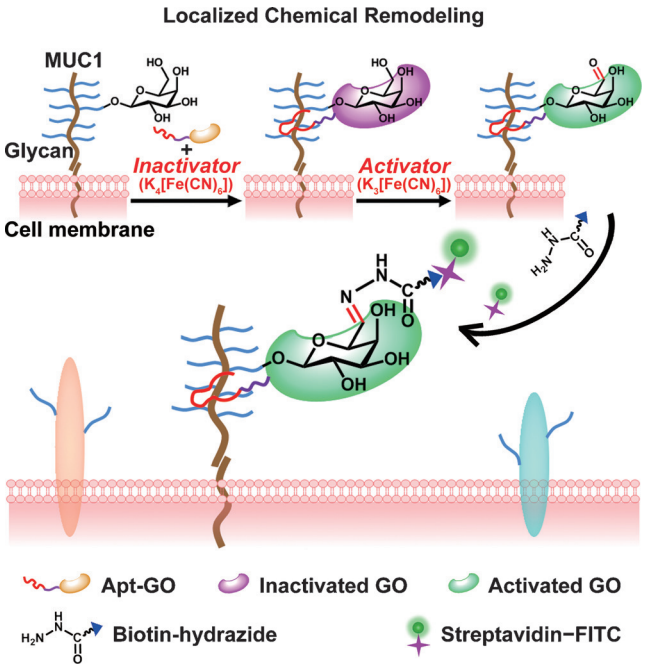


***Scheme 1.*** Representation of the localized chemical remodeling (LCM) strategy for live cell imaging of protein-specific glycoform.

abnormal neoplastic progression.[1,8] The achievement of LCM requires MUC1-targeting and terminal Gal/GalNAc-transforming assay components. S2.2[9] (Apt) is a 25-mer DNA aptamer that exhibits the highest binding affinity to date toward MUC1 VNTR region. Gal oxidase (GO)[10] is a copper metalloenzyme capable of effecting oxidation of C6-hydroxy group of terminal Gal/GalNAc to the corresponding aldehyde. GO can be switched between the off and on states by using $K_4[Fe(CN)_6]$ inactivator and $K_3[Fe(CN)_6]$ activator, respectively.[11] An Apt-GO conjugate, comprised of Apt and GO, can therefore be used for LCM and MUC1-specific imaging of terminal Gal/GalNAc (Scheme 1): Apt delivery of off-state GO (inactivated by $K_4[Fe(CN)_6]$) to the cell surface MUC1 site, switch-on of GO activity (activated by $K_3[Fe(CN)_6]$) for proximity catalysis-enabled generation of aldehyde on MUC1-bound Gal/GalNAc termini, bioorthogonal labeling (that is, hydrazone ligation with biotin hydrazide[10d,12] and recognition with streptavidin-FITC), and imaging. It is important to note that the small size of Apt[4d] ensures the confinement of catalysis event in a protein-specific manner.

With the LCM scheme designed, we proceeded to the fabrication of Apt-GO. The conjugation is accomplished by an amide bond formation between amino group of a 5′-amino-derivatized Apt ($Apt\text{-}NH_2$) and surface-exposed carboxyl group of GO, with unreacted $Apt\text{-}NH_2$ removed by ultrafiltration. Reaction with GO using 3′-FAM-functionalized $Apt\text{-}NH_2$ ($FAM\text{-}Apt\text{-}NH_2$) under otherwise identical conditions confirms successful covalent conjugation (synthesis of FAM-Apt-GO in this case), as evidenced by sodium dodecyl sulfate–polyacrylamide gel electrophoresis (SDS-PAGE; Supporting Information, Figure S1): a band exhibiting both FAM fluorescence and Coomassie blue staining capacity and with a slightly higher molecular weight than GO can be cleanly observed. The specific recognition capability of Apt toward MUC1 is retained after GO conjugation, as verified on MCF-7 (MUC1-positive) and HepG2 (MUC1-negative) cells[4d] (Supporting Information, Figure S2): neither MCF-7 cells nor HepG2 cells show any fluorescence upon incubation with a 5′-FAM-functionalized random-sequenced DNA (Ran-FAM); both 5′-FAM-derivatized Apt (Apt-FAM) and FAM-Apt-GO light up MCF-7 cells but not HepG2 cells under 488 nm excitation by confocal laser scanning microscopy (CLSM).

The feasibility of using LCM for live cell imaging of protein-specific glycoform is then evaluated on MCF-7 cells. As expected, GO can effect GCM of Gal/GalNAc on the whole cell surface and further bioorthogonal labeling (reaction with biotin hydrazide for 1.5 h and streptavidin-FITC for 0.5 h) allows the observation of FITC fluorescent signal at the MCF-7 cell periphery (Figure 1, bottom left). The same type

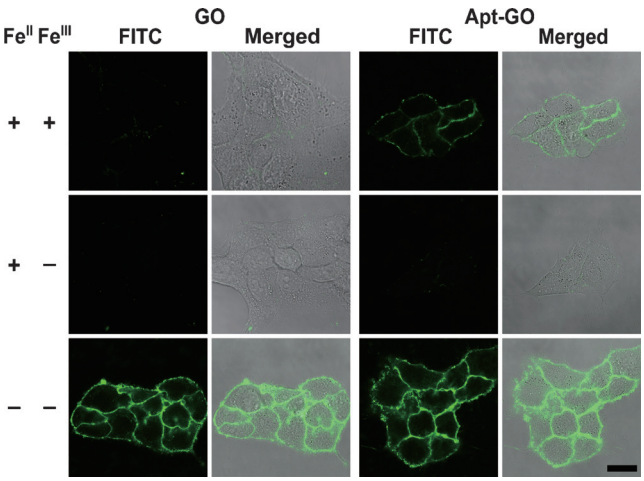


***Figure 1.*** Demonstration of the feasibility of using LCM for live cell imaging of MUC1-bound terminal Gal/GalNAc. CLSM images of MCF-7 cells after 1) treatment with either GO or Apt-GO (without or with $K_4[Fe(CN)_6]$) and washing, 2) no treatment or treatment with $K_3[Fe(CN)_6]$ followed by washing, and 3) bioorthogonal labeling. Excitation wavelength for FITC fluorescence images: 488 nm; Imaging window: 500–565 nm. Scale bar: 20 μm.

of FITC fluorescent signal can be identified by the replacement of GO with Apt-GO, confirming the retention of GO activity in Apt-GO (Figure 1, bottom right). The optimum GO concentration for subsequent imaging applications is determined to be 100 $\mu g\,mL^{-1}$, as judged by the minimum amount of GO required to reach the plateau FITC signal intensity (Supporting Information, Figure S3). GO inactivation is a prerequisite for strictly eliminating GCM during the Apt affinity binding process. Quantitative measurement of GO activity as a function of $K_4[Fe(CN)_6]$ inactivator concentration suggests 100 mM as the ideal concentration (Supporting Information, Figure S4). At this concentration, the GO activity has essentially reached the minimum level and the inactivation effect remains even after subsequent removal of $K_4[Fe(CN)_6]$. Thus, with GO inactivation performed before incubation with MCF-7 cells, neither GO (Figure 1, middle

  

left) nor Apt-GO (Figure 1, middle right) in the off state can catalyze Gal/GalNAc oxidation and therefore, no reactive handle is available for bioorthogonal labeling and fluorescent imaging. The activation of GO activity by $K_3[Fe(CN)_6]$ activator has been experimentally validated previously[11] and can indeed be used in the LCM setting (Supporting Information, Figure S5). Taken together, LCM as a MUC1-specific terminal Gal/GalNAc imaging tool (Figure 1, top right) can be achieved by 1) inactivation of Apt-GO with 100 mM $K_4[Fe(CN)_6]$, 2) incubation with MCF-7 cells for 0.5 h, 3) extensive washing with phosphate buffer saline (10 mM, pH 7.4) to remove excess Apt-GO and $K_4[Fe(CN)_6]$, and 4) reactivation of Apt-GO for 0.5 h with 10 mM $K_3[Fe(CN)_6]$ for catalyzing Gal/GalNAc oxidation. A notable assay feature for the LCM approach as compared with the MOE method[5] is substantially shortened time required for chemical transformation (1–2 h versus 48 h[4d,e]). LCM is responsible for the generation of FITC signal as without Apt-GO, no FITC signal as a result of nonspecific adsorption of either biotin hydrazide or streptavidin-FITC can be observed in the absence or presence of either $K_4[Fe(CN)_6]$ or $K_3[Fe(CN)_6]$ (Supporting Information, Figure S6). A high cell viability, as determined from MTT assay, is maintained throughout the LCM process and upon extended further cell culturing (Supporting Information, Figure S7). MUC1-targeting Apt is required for the successful implementation of LCM, as without Apt, GO is removed at the washing step and no Gal/GalNAc oxidation occurs on MCF-7 cell surface (Figure 1, top left).

To confirm that MUC1-bound terminal Gal/GalNAc is the specific site undergoing LCM, three sets of experiments were performed (Figure 2). The MUC1 glycosylation is *O*-linked and therefore, inhibition of *N*-glycosylation pathways should not affect the overall LCM efficiency. Treatment with tunicamycin,[4e] a reagent that can block the formation of protein *N*-glycosidic linkages, indeed does not lead to apparent change in the cellular FITC signal intensity when compared with the untreated cells (Figure 2A, top and middle). The carbohydrate remodeling site specificity is confirmed based on the rationale that if Gal/GalNAc is the target reaction site, one should be able to inhibit LCM by blocking GO activity with externally added D-Gal. Thus, MCF-7 cells are challenged with Apt-GO in the presence of excess D-Gal. Indeed, the FITC signal intensity is markedly decreased (Figure 2A, top and bottom), supporting Gal/GalNAc as the LCM site. The protein site specificity is verified by Western blot analysis on MCF-7 cells after LCM and reaction with biotin hydrazide. An anti-MUC1 antibody and an antibiotin antibody are used, respectively, to target MUC1 and Gal/GalNAc-linked biotin. A single band shows up simultaneously on both anti-MUC1 and antibiotin membranes (Figure 2B), indicating that Gal/GalNAc undergoing oxidation is located specifically on MUC1-bound glycans. As a control and as expected, no band appears on the antibiotin membrane for the pristine MCF-7 cells (Figure 2B). To further demonstrate protein site specificity, six glycoproteins, including three glycoproteins bearing experimentally confirmed terminal Gal/GalNAc (transferrin receptor,[13a–c] Hsp90 α,[13b,d,e] annexin II[13b,d,f]) (Supporting Information,

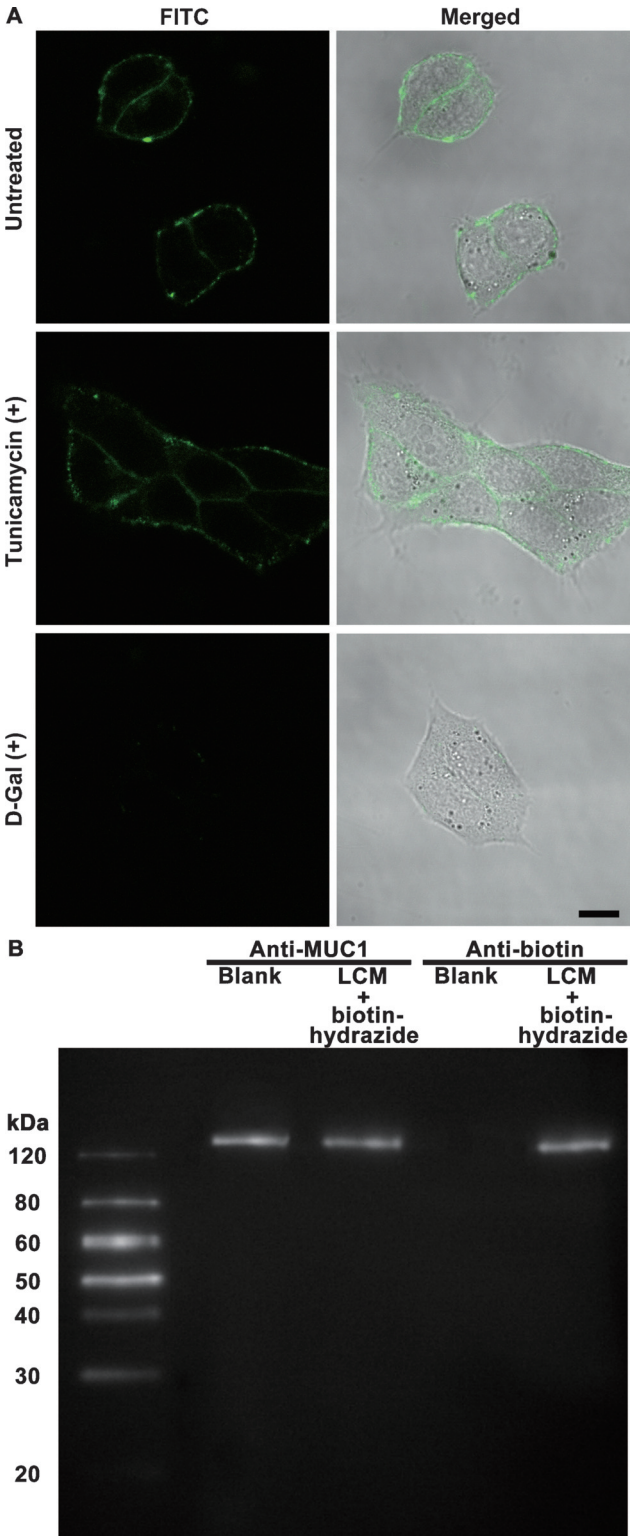


***Figure 2.*** Demonstration of MUC1-bound terminal Gal/GalNAc as the LCM site. A) CLSM images of MCF-7 cells after LCM and bioorthogonal labeling (top), tunicamycin-treated MCF-7 cells after LCM and bioorthogonal labeling (middle), and MCF-7 cells after LCM and bioorthogonal labeling, with D-Gal added at the $K_3[Fe(CN)_6$ incubation step (bottom). Scale bar: 10 μm. B) Western blot diagram of cell lysates of pristine MCF-7 cells (blank) and MCF-7 cells after LCM and reaction with biotin hydrazide. Left lane: molecular weight markers; Middle two lanes: with anti-MUC1 antibody; Right two lanes: with antibiotin antibody.

  

Figure S8) and three regularly encountered glycoproteins (integrin α5,[13g] ENO1,[13b,f] Hsp27[13b]) (Supporting Information, Figure S9), are purified with immunoprecipitation, and none of these glycoproteins are modified under LCM condition. As an additional control, MCF-7 cells undergoing direct treatment with GO identifies multiple bands on the antibiotin membrane (Supporting Information, Figure S10), suggesting the occurrence of non-selective modification. Consistent with this, immunoprecipitation purification of the aforementioned six glycoproteins from GO-treated MCF-7 cells shows that all these glycoproteins have been modified (Supporting Information, Figures S11, S12). Taken together, the stringent separation of binding and catalysis events, together with the small size of Apt, ensures the efficient achievement of LCM. Significantly, these site-specificity verification experiments have also established LCM as an effective molecular ruler between MUC1 and Gal/GalNAc because only Gal/GalNAc at the immediate vicinity of MUC1 can react and generate reactivity-based signal.

As a demonstration of the utility of the LCM protocol, quantitative analysis of protein-specific glycoform was performed. To this end, the expression level of MUC1-bound terminal Gal/GalNAc is measured for MCF-7 and T47D cells. Qualitatively, the FITC signal of MCF-7 cells is apparently stronger than that of T47D cells (Figure 3 A). Quantitatively, the FITC signal intensity obtained from pixel readout of CLSM images is 22.8 ± 2.4 for MCF-7 cells and 9.5 ± 1.0 for T47D cells (Figure 3 B). The MCF-7 to T47D relative ratio of expression level of MUC1-bound terminal Gal/GalNAc can therefore be calculated as 2.4.

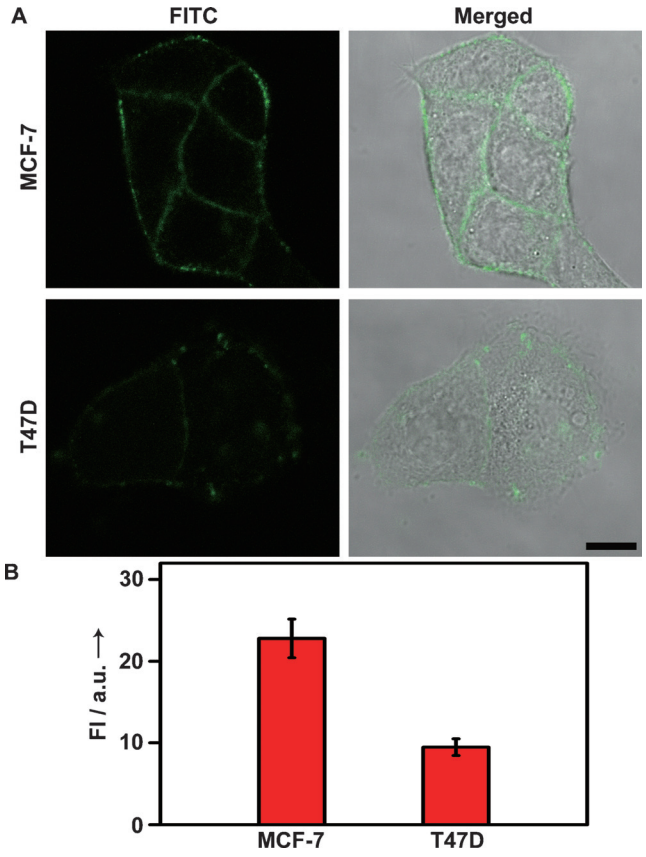


***Figure 3.*** Quantitative analysis of MUC1-bound terminal Gal/GalNAc across different cell lines using LCM strategy and CLSM. A) CLSM images of MCF-7 and T47D cells after LCM and bioorthogonal labeling. Scale bar: 10 μm. B) The average value of fluorescence signal intensity at the periphery of MCF-7 and T47D cells from CLSM images. Data are represented as average ± standard deviation (from five independent measurements).

The quantitative information on MUC1-bound terminal Gal/GalNAc can also be collected with a high-throughput signal readout method, that is, flow cytometry (FCM). The average FITC signal intensity is higher for MCF-7 cells compared with T47D cells, with a relative ratio of 2.8 (Figure 4, left), which agrees with the value from CLSM images. The quantitative information acquired for MUC1

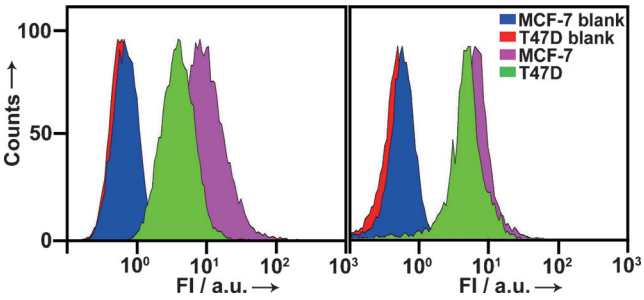


***Figure 4.*** Quantitative analysis of MUC1-bound terminal Gal/GalNAc and MUC1 across different cell lines using LCM strategy and FCM. FCM results for MCF-7 and T47D cells after either LCM and bioorthogonal labeling (left) or incubation with Apt-FAM (right). MCF-7 blank and T47D blank represent no treatment.

through the binding of Apt-FAM shows an MCF-7 to T47D relative ratio of 1.4 (Figure 4, right). Therefore, the MCF-7 to T47D relative ratio of expression level of MUC1-bound terminal Gal/GalNAc per MUC1 chain is determined to be 2.0, which is in good agreement with the literature reported value.[14] These results confirm the validity of using LCM for distinguishing different cell phenotypes.

In conclusion, we have proposed a distinct LCM strategy and demonstrated its utility as a tool for efficient and reliable access to protein-specific glycoform information. Compared with currently used MOE method, desired assay features associated with LCM approach include minimum target cell perturbation, short reaction timeframe, effectiveness as a molecular ruler, and quantitative analysis capability. Given the ever-expanding available repertoire of protein-binding aptamers[15] and carbohydrate-processing enzymes,[10c,16] the LCM strategy should be easily adaptable to the live cell imaging of a wide range of protein-specific glycoforms.

## Acknowledgements

We gratefully acknowledge support from the National Natural Science Foundation of China (21675082, 21635005), the National Basic Research Program (2014CB744501), and State Key Laboratory of Analytical Chemistry for Life Science (5431ZZXM1608).

  

## Conflict of interest

The authors declare no conflict of interest.

**Keywords:** live cell imaging · localized chemical remodeling · molecular ruler · protein-specific glycoform · proximity catalysis

**How to cite:** *Angew. Chem. Int. Ed.* **2017**, *56*, 8139–8143
*Angew. Chem.* **2017**, *129*, 8251–8255

[1] S. R. Stowell, T. Ju, R. D. Cummings, *Annu. Rev. Pathol.* **2015**, *10*, 473–510.
[2] a) F. Bard, J. Chia, *Trends Cell Biol.* **2016**, *26*, 379–388; b) R. Raman, S. Raguram, G. Venkataraman, J. C. Paulson, R. Sasisekharan, *Nat. Methods* **2005**, *2*, 817–824; c) M. A. Wolfert, G. J. Boons, *Nat. Chem. Biol.* **2013**, *9*, 776–784.
[3] a) A. Almeida, D. Kolarich, *Biochim. Biophys. Acta-Gen. Subj.* **2016**, *1860*, 1583–1595; b) C. A. Reis, H. Osorio, L. Silva, C. Gomes, L. David, *J. Clin. Pathol.* **2010**, *63*, 322–329.
[4] a) Y. Haga, K. Ishii, K. Hibino, Y. Sako, Y. Ito, N. Taniguchi, T. Suzuki, *Nat. Commun.* **2012**, *3*, 907; b) F. Doll, A. Buntz, A.-K. Späte, V. F. Schart, A. Timper, W. Schrimpf, C. R. Hauck, A. Zumbusch, V. Wittmann, *Angew. Chem. Int. Ed.* **2016**, *55*, 2262–2266; *Angew. Chem.* **2016**, *128*, 2303–2308; c) B. Belardi, A. de la Zerda, D. R. Spiciarich, S. L. Maund, D. M. Peehl, C. R. Bertozzi, *Angew. Chem. Int. Ed.* **2013**, *52*, 14045–14049; *Angew. Chem.* **2013**, *125*, 14295–14299; d) N. Wu, L. Bao, L. Ding, H. Ju, *Angew. Chem. Int. Ed.* **2016**, *55*, 5220–5224; *Angew. Chem.* **2016**, *128*, 5306–5310; e) W. Lin, Y. Du, Y. Zhu, X. Chen, *J. Am. Chem. Soc.* **2014**, *136*, 679–687.
[5] a) S. H. Rouhanifard, L. U. Nordstrom, T. Zheng, P. Wu, *Chem. Soc. Rev.* **2013**, *42*, 4284–4296; b) P. V. Robinson, G. de Almeida-Escobedo, A. E. de Groot, J. L. McKechnie, C. R. Bertozzi, *J. Am. Chem. Soc.* **2015**, *137*, 10452–10455.
[6] a) P. V. Chang, X. Chen, C. Smyrniotis, A. Xenakis, T. Hu, C. R. Bertozzi, P. Wu, *Angew. Chem. Int. Ed.* **2009**, *48*, 4030–4033; *Angew. Chem.* **2009**, *121*, 4090–4093; b) S. T. Laughlin, C. R. Bertozzi, *Nat. Protoc.* **2007**, *2*, 2930–2944; c) S. J. Luchansky, S. Argade, B. K. Hayes, C. R. Bertozzi, *Biochemistry* **2004**, *43*, 12358–12366.
[7] a) C. L. Hattrup, S. J. Gendler, *Annu. Rev. Physiol.* **2008**, *70*, 431–457; b) D. W. Kufe, *Oncogene* **2013**, *32*, 1073–1081.
[8] G. Ashwell, J. Harford, *Annu. Rev. Biochem.* **1982**, *51*, 531–554.
[9] a) C. S. M. Ferreira, C. S. Matthews, S. Missailidis, *Tumor Biol.* **2006**, *27*, 289–301; b) Z. Fan, L. Sun, Y. Huang, Y. Wang, M. Zhang, *Nat. Nanotechnol.* **2016**, *11*, 388–394.
[10] a) K. Parikka, E. Master, M. Tenkanen, *J. Mol. Catal. B* **2015**, *120*, 47–59; b) J. W. Whittaker, *Chem. Rev.* **2003**, *103*, 2347–2363; c) K. K. Palaniappan, C. R. Bertozzi, *Chem. Rev.* **2016**, *116*, 14277–14306; d) T. N. C. Ramya, E. Weerapana, B. F. Cravatt, J. C. Paulson, *Glycobiology* **2013**, *23*, 211–221.
[11] J. W. Whittaker, *Arch. Biochem. Biophys.* **2005**, *433*, 227–239.
[12] J. E. McCombs, J. J. Kohler, *Bioconjugate Chem.* **2016**, *27*, 1013–1022.
[13] a) C. Steentoft, S. Y. Vakhrushev, H. J. Joshi, Y. Kong, M. B. Vester-Christensen, K. T. B. G. Schjoldager, K. Lavrsen, S. Dabelsteen, N. B. Pedersen, L. Marcos-Silva, R. Gupta, E. P. Bennett, U. Mandel, S. Brunak, H. H. Wandall, S. B. Levery, H. Clausen, *EMBO J.* **2013**, *32*, 1478–1488; b) T.-Y. Yen, B. A. Macher, C. A. McDonald, C. Alleyne-Chin, L. C. Timpe, *J. Proteome Res.* **2012**, *11*, 656–667; c) G. R. Hayes, C. A. Enns, J. J. Lucas, *Glycobiology* **1992**, *2*, 355–359; d) J. Saint-Guirons, E. Zeqiraj, U. Schumacher, P. Greenwell, M. Dwek, *Proteomics* **2007**, *7*, 4082–4089; e) L. Ermini, J. Bhattacharjee, A. Spagnoletti, N. Bechi, S. Aldi, C. Ferretti, L. Bianchi, L. Bini, F. Rosati, L. Paulesu, F. Ietta, *Am. J. Physiol. Cell Physiol.* **2013**, *305*, C931–C940; f) S. A. Whelan, M. Lu, J. He, W. Yan, R. E. Saxton, K. F. Faull, J. P. Whitelegge, H. R. Chang, *J. Proteome Res.* **2009**, *8*, 4151–4160; g) H. Nakagawa, M. Zheng, S.-i. Hakomori, Y. Tsukamoto, Y. Kawamura, N. Takahashi, *Eur. J. Biochem.* **1996**, *237*, 76–85.
[14] S. Muller, F. G. Hanisch, *J. Biol. Chem.* **2002**, *277*, 26103–26112.
[15] M. R. Gotrik, T. A. Feagin, A. T. Csordas, M. A. Nakamoto, H. T. Soh, *Acc. Chem. Res.* **2016**, *49*, 1903–1910.
[16] J. B. Rannes, A. Ioannou, S. C. Willies, G. Grogan, C. Behrens, S. L. Flitsch, N. J. Turner, *J. Am. Chem. Soc.* **2011**, *133*, 8436–8439.

Manuscript received: April 1, 2017
Accepted manuscript online: May 29, 2017
Version of record online: June 12, 2017

  